ACS OMEGA

Open Access

http://pubs.acs.org/journal/acsodf

Article

Curcumin-Loaded ZIF-8 Nanomaterials: Exploring Drug Loading Efficiency and Biomedical Performance

Mahbubur Rahman, Mohashin Kabir, Tarikul Islam, Yafei Wang, Qi Meng, Hailei Liu, Shaojuan Chen,* and Shaohua Wu*

Cite This: *ACS Omega* 2025, 10, 3067−3079

Read Online

ACCESS | Metrics & More | Article Recommendations

ABSTRACT: Curcumin (cur) possesses excellent therapeutic properties, including anti-inflammatory, antioxidant, and healing-promoting effects. However, its biomedical application is impeded by its rapid degradation, limited bioavailability, and poor aqueous solubility. Zeolitic imidazole framework (ZIF-8), with a high surface area and tunable pore size, is designed and used as a cur delivery carrier to overcome these limitations. The synthesis of cur-loaded ZIF-8 involves a solvothermal method, followed by encapsulation of cur within the porous structure of ZIF-8. The amount of cur was varied to synthesize a series of panel cur-loaded ZIF-8. 0.5 mg/mL cur@ZIF-8 that showed higher drug loading efficiency (85.91 ± 1.26%) and drug loading capability (12.93 ± 0.19%) without changes in shape, size, crystallinity, chemical composition, and thermal stability of original ZIF-8. 0.5 mg/mL cur@ZIF-8 exhibited excellent surface area (1591.02 m^2/g) and micropore volume (0.54 cm^3/g). Cur@ZIF-8 demonstrated superior thermal stability and outstanding antibacterial properties, achieving 99% efficiency compared with free cur. It exhibited less cytotoxicity against human fibroblast cells and better antioxidant properties than ZIF-8. Furthermore, the drug release rate of cur@ZIF-8 is higher under acidic conditions, which promotes wound healing due to the acidic microenvironment of the skin. The biocompatibility and stability of cur@ZIF-8 nanoparticles highlight their potential as promising candidates for diverse biomedical applications.

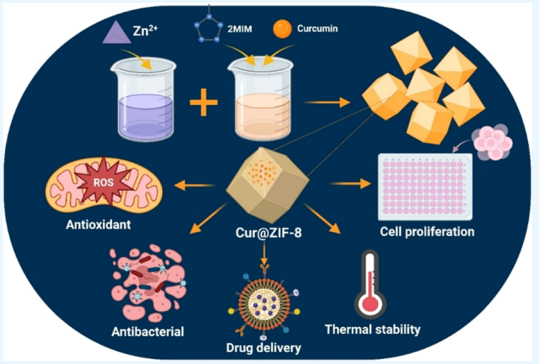

1. INTRODUCTION

In nanotechnology and materials science, combining traditional medicinal compounds with advanced material frameworks has opened new paths for biomedical applications.[1] One such intriguing combination is the incorporation of curcumin (cur), a bioactive compound from the turmeric plant, into metal−organic frameworks (MOFs). Cur is a lipophilic polyphenol that is chemically identified as 1,7-bis(4-hydroxy-3-methoxyphenyl)-hepta-1,6-diene-3,5-dione. Several clinical, in vivo and in vitro, experiments have indicated that cur possesses antioxidant, anticancer, anti-inflammatory, and wound healing properties.[2,3] It is also highly biocompatible and biodegradable.[4,5] However, cur cannot be delivered systemically because of its limited bioavailability, high hydrophobicity, and extensive first-pass metabolism. Previous research has demonstrated that cur can be dispersible in aqueous media by encapsulating it in inorganic-based carriers like silica,[6−8] gold,[9,10] and silver[11−13] nanoparticles (NPs) or organic-based carriers such as cyclodextrin,[14,15] micelles,[16,17] liposomes,[18,19] niosomes,[20,21] and cubosomes[22,23] NPs. However, the synthesis of these NPs was tedious and laborious. Thus, developing an easy-to-follow and effective technology for cur encapsulation into nanocarriers is greatly desired.

MOFs as drug carriers have been demonstrated in numerous groundbreaking studies in recent years. MOFs are a form of nanostructured and nanoporous material that is relatively new and is composed of inorganic metal nodes that are connected by organic linkers.[24,25] MOFs are endowed with numerous advantageous characteristics, such as ultrahigh porosity (94% free volume of MOF-399), homogeneous cavities that are tunable, and extremely high surface areas (10,400 $m^2\ g^{-1}$ of MOF-200). Moreover, MOFs can be precisely customized by modifying the geometries of organic linkers and coordination modes of inorganic metal ions to achieve the specific functions and performances needed.[26] MOFs have been extensively investigated to determine their functional applications in a variety of disciplines, including gas storage,[27,28] catalysis,[29−32] separation,[33,34] energy storage,[35−37] sensing,[38,39] drug delivery,[40−43] and so on. The zeolitic imidazolate framework-8

Received: October 31, 2024
Revised: December 26, 2024
Accepted: December 30, 2024
Published: January 14, 2025

(ZIF-8) is an MOF that is composed of zinc ions and 2-methyl imidazole (2MIM).[44] Previous research has demonstrated that ZIF-8 is a highly preferred method for drugs, including doxorubicin,[45−47] 5-florouracil,[48−50] lysozyme,[51−53] and rapamycin.[54,] While several groups tried to add the drug to ZIF-8, their progress was hindered by the drug's poor stability in biological environments and reduced loading.

In this research, a straightforward nanoprecipitation process was established to synthesize water-dispersible cur-loaded ZIF-8 (cur@ZIF-8) NPs. A series of cur@ZIF-8 was synthesized by varying the amount of cur, such as 0.1, 0.3, 0.5, 1, and 2 mg/mL concerning solvent amount. The Brunauer−Emmett−Teller (BET) test was performed to determine the specific surface areas and micropore volume. Furthermore, thermogravimetric analysis (TGA) studies will provide insights into cur@ZIF-8's thermal stability. The drug loading efficiency (DLE) and drug loading capacity (DLC) of cur@ZIF-8 were quantified. In the biomedical context, cur@ZIF-8 is hypothesized to control drug release and enhance cell proliferation, antibacterial activity, and antioxidant activity. The potential of cur@ZIF-8 is to serve as a multifunctional platform for targeted drug delivery.

This research aims to advance our understanding of the MOF-based drug delivery process and pave the way for the development of novel nanotherapeutics with enhanced clinical outcomes. This study presents a detailed exploration of the synthesis, characterization, and biomedical applications of cur@ZIF-8. By integrating the therapeutic potential of cur with the innovative properties of ZIF-8, this research aims to contribute to the growing field of nanomedicine and offer new perspectives for the treatment of various diseases.

2. EXPERIMENTAL SECTION

2.1. Materials. Cur (M_w = 368.39) was purchased from Shanghai Macklin Biochemical Technology Co., Ltd. Zinc acetate anhydrous ($Zn(Ac)_2.6H_2O$), 2-methyl imidazole (2-MIM), methanol, ethanol, and hydrochloric acid (HCl) were collected from Sinopharm Chemical Reagent Company Limited (China). 1,1-Diphenyl-2-picrylhydrazyl (DPPH) was obtained from Yesen Biotechnology Company Limited (China), and 3-(4,5-dimethylthiazol-2-yl)-2,5-diphenyltetrazolium bromide (MTT, purity = 98%) was purchased from Sigma-Aldrich. There was no further modification of any chemical reagents used in this research.

2.2. Synthesis of Cur-Loaded ZIF-8. ZIF-8 and various amounts of cur-loaded ZIF-8 were synthesized using a one-pot synthesis technique according to the literature[56] with slight modifications. In Solution A, $Zn(Ac)_2.6H_2O$ was dissolved in deionized (DI) water at a concentration of 30 mg/mL. 2-MIM and cur were dissolved in methanol simultaneously at concentrations of 33 and 0.1, 0.3, 0.5, 1, and 2 mg/mL, respectively, resulting in Solution B. The volume ratio of Solution B to Solution A was 2:1. Afterward, the two solutions were vigorously stirred and mixed for 60 s at 700 rpm (RPM). The mixture was centrifugated at 8000 rpm for 15 min and washed three times with methanol. After freeze-drying methods, the final product obtained was cur-loaded ZIF-8, also known as 0.1, 0.3, 0.5, 1, and 2 mg/mL cur@ZIF-8. ZIF-8 was synthesized in its original form using a similar method, except that cur was not present in Solution B. The amounts of various ingredients for the synthesis of ZIF-8 and 0.1, 0.3, 0.5, 1, and 2 mg/mL cur@ZIF-8 are presented in Table 1.

Table 1. Ingredients Amount for the Synthesis of Cur@ZIF-8

	Solution A		Solution B		
sample name	$Zn(Ac)_2$ (g)	DI water (mL)	2-MIM (g)	Cur (mg)	methanol (mL)
ZIF-8	1.20	40	2.64	0	80
0.1 mg/mL cur@ZIF-8	1.20	40	2.64	8	80
0.3 mg/mL cur@ZIF-8	1.20	40	2.64	24	80
0.5 mg/mL cur@ZIF-8	1.20	40	2.64	40	80
1 mg/mL cur@ZIF-8	1.20	40	2.64	80	80
2 mg/mL cur@ZIF-8	1.20	40	2.64	160	80

2.3. Characterization. *2.3.1. Surface Morphology.* The morphology and structure of ZIF-8 and various concentrations (0.1, 0.3, 0.5, 1, and 2 mg/mL) of cur@ZIF-8 were analyzed by using scanning electron microscopy (SEM, TESCAN VEGA3, Czech Republic) and transmission electron microscopy (TEM). Initially, appropriate amounts of ZIF-8 and cur@ZIF-8 were dispersed in methanol. For SEM analysis, the ZIF-8 and cur@ZIF-8 methanol solutions were dropped onto the silicon water and dried. The silicon water was then attached to the SEM holder using conductive adhesive. Before SEM imaging, a gold coating was applied to the surface of the samples for 1 min to enhance conductivity. For TEM analysis, the ZIF-8 and cur@ZIF-8 methanol solutions were dropped onto a copper grid and dried thoroughly before observation. The surface morphology of the samples was examined, and then, the size of ZIF-8 and cur@ZIF-8 particles were determined using ImageJ software (National Institutes of Health, NIH).

2.3.2. X-ray Diffraction. XRD patterns of ZIF-8, cur, and cur@ZIF-8 concentrations of 0.1, 0.3, 0.5, 1, and 2 mg/mL were obtained on a Rigaku Ultima IV instrument (Japan) equipped with a Cu Kα radiation source. As part of the setup, the machine was configured to operate at a voltage of 30 kV, a current of 30 mA, and a scanning range of 5−60° (2θ).

2.3.3. Fourier Transform Infrared Radiation. The FTIR spectra and chemical groups of ZIF-8, cur, and various concentrations of cur@ZIF-8 (0.1, 0.3, 0.5, 1, and 2 mg/mL) were recorded by using a Fourier transform infrared radiation analyzer (Thermo Fisher Scientific 5225 Verona RD). The scanning frequency, wavenumber range, and resolution were 32/min, 4000−400, and 2 cm^{-1}, respectively.

2.3.4. Drug Loading Capacity and Drug Loading Efficiency. The DLC and DLE are crucial parameters in drug delivery systems, indicating the amount of drug that can be incorporated into a carrier. Generally, DLC and DLE percentages are calculated using equations (eqs 1 and 2).

DLC refers to the maximum amount of drug that can be loaded onto a carrier or delivery system. It represents the percentage of the total weight of the carrier and drug that is occupied by the carrier

$$\text{DLC}\ (\%) = \frac{\text{amount of cur loaded}}{\text{total amount of cur@ZIF-8}} \times 100 \quad (1)$$

DLE is a measure of how efficiently the drug is loaded onto the carrier, indicating the percentage of the drug successfully

https://doi.org/10.1021/acsomega.4c09945
ACS Omega 2025, 10, 3067−3079

incorporated. It represents the percentage of the initially added drug that is effectively loaded onto the carrier.

$$\text{DLE}\ (\%) = \frac{\text{amount of cur loaded in ZIF-8}}{\text{amount of cur initially used}} \times 100 \quad (2)$$

2.3.5. Surface Area and Pore Characteristics. The BET test was performed to determine the specific surface areas and pore characteristics of ZIF-8 and cur@ZIF-8. A 12 h vacuum degassing was conducted at 150 °C on samples of ZIF-8 and cur@ZIF-8 before the measurement to remove any adsorption of moisture or gases. The analysis was conducted using a BET surface area analyzer (Hou Kaiqi, China) with nitrogen as the adsorbate at −196 °C. Sample holders were filled with approximately 50 mg of each sample, and nitrogen adsorption−desorption isotherms were obtained by incrementally increasing the relative pressure (P/P_0) from 0 to 1.

2.3.6. Thermogravimetric Analysis. Using a thermal analyzer (STA449 F3 Jupiter, Germany), the thermal characteristics of ZIF-8, cur, and 0.5 mg/mL cur@ZIF-8 were investigated in a nitrogen environment at ambient temperature and 800 °C at a heating rate of 10 °C/min.

2.3.7. Drug Release and Kinetics Model. The actual loading amount of cur in 0.5 mg/mL cur@ZIF-8 was measured before the drug release test; 5 mg of 0.5 mg/mL cur@ZIF-8 was dissolved in 1 mL of 1 M HCl and then diluted with ethanol. The quantity of dissolved cur was then evaluated by a microplate spectrophotometer (Tecan M200 Pro, Switzerland) at 431 nm. The cur drug-release profile was investigated according to reference[57] with some modifications. After the samples were carefully weighed and submerged in 1.0 mL of PBS solution at pH 7.4 and 5.4, they were placed in a shaker maintained at 37 °C at 80 rpm. Tecan M200 Pro was used to evaluate the cumulative release of cur at different time points (1, 2, 4, 6, 12, 24, ···, 120 h). An aliquot of 1.0 mL PBS was withdrawn at predetermined time points, followed by an addition of 1.0 mL of fresh PBS. Each sample was measured in triplicate, and results were presented as mean standard deviation (SD) concerning eq 3.

$$\text{cumulative cur release}\ (\%) = (m_1 + m_2 + m_3 + \ldots + m_n)/M \times 100 \quad (3)$$

where m_n (n = 1, 2, 3, ···) was the mass cur in PBS at a predetermined time and M referred to the actual amount of cur loaded in the cur@ZIF-8.

In order to determine which model was appropriate, zero-order, first-order, Higuchi, Korsmeyer-Peppas (K−P), and Hixson-Crowell (H−C) models were used to fit the release kinetics of cur from cur@ZIF-8 at pH 7.4 and 5.4. Drug release kinetics describes how a drug is released from a material over time and can be modeled mathematically. Here is a brief overview of five common drug release kinetic models (eqs 4−8).

zero-order model:

$$Q_t = Q_0 + k_0 t \quad (4)$$

first-order model:

$$\log Q_t = \log Q_0 - k_1 t \quad (5)$$

Higuchi model:

$$Q_t = k_H \cdot t^{1/2} \quad (6)$$

Korsmeyer−Peppas model:

$$Q_t/Q_\infty = k_K \cdot t^n \quad (7)$$

Hixson−Crowell model:

$$W_0^{1/3} - W_t^{1/3} = k_{HC} \cdot t \quad (8)$$

where Q_t is the cumulative amount of drug released at time t, Q_0 is the initial amount of drug, n is the release exponent of the K−P model, $W_0^{1/3}$ is the initial cubic root of the drug remaining amount, and $W_t^{1/3}$ is the cubic root of the drug remaining amount at time t. The release constants of the zero-order, first-order, Higuchi, K−P, and H−C models are denoted as k_0, k_1, k_H, k_K, and k_{HC}, respectively. Controlled release formulations can be better understood and optimized by using these models.

2.3.8. Antioxidant Test. The DPPH assay was performed according to the literature[58] with slight modifications to evaluate the antioxidant capacities of ZIF-8, cur@ZIF-8 (0.5 mg/mL), and cur. Antioxidants, whether produced naturally or synthetically, can prevent harmful unintended reactions by reducing the DPPH radical, which changes its color from deep violet to purple.[59] To prepare the DPPH solution, 0.004 g of DPPH was accurately weighed and dissolved in 100 mL of methanol in a conical flask. This solution was then stored in a dark environment to prevent degradation. For the test samples, 5 mg each of ZIF-8, cur@ZIF-8, and cur were weighed and dissolved in 20 mL of methanol to prepare a 250 μg/mL stock solution. This stock solution was diluted to obtain concentrations of 12.5, 25, 50, 100, 150, 200, and 250 μg/mL. Equal volumes of the sample solution and the DPPH solution were mixed. Pure methanol was added to the DPPH solution as a blank control. After an appropriate incubation period, the absorbance at 517 nm was measured using a Tecan M200 Pro. The radical scavenging activity (RSA) was then calculated using eq 9.

$$\text{RSA}\ (\%) = (A_0 - A_S)/A_0 \times 100 \quad (9)$$

where A_0 and A_S were the absorbance values of the blank control and the absorbance values of samples, respectively.

All the concentrations of the sample were plotted on the X axis, and the RSA (%) was plotted on the Y axis by data analysis process at a 95% confidence level through the regression equation of the 50% inhibitions concentration (IC_{50}) value of cur and 0.5 mg/mL cur@ZIF-8 was calculated.

2.3.9. In Vitro Cell Viability. The 3-[4,5-dimethylthiazol-2-yl]-2,5-diphenyltetrazolium bromide (MTT) assay was employed to evaluate the cytotoxicity and cell proliferation of ZIF-8, cur@ZIF-8, and cur against human dermal fibroblast cells (HDFs) from the cell bank of the Chinese Academy of Sciences in China. The samples were sterilized under exposure to ultraviolet (UV) light for 2 h and inserted into a 96-well plate at the appropriate weight. The concentrations of cur@ZIF-8, cur, and ZIF-8 were 100, 112.93, and 12.93 μg/mL, respectively. The cell culture medium was prepared by mixing 89% Dulbecco's Modified Eagle Medium (DMEM), 10% fetal bovine serum (FBS), and 1% penicillin-streptomycin (P/S) solution. Cell attachment was achieved by seeding the sterilized nanoparticles with cultured cells at a density of 1×10^3 cells/well and incubating them at 37 °C in a 5% v/v CO_2 environment for 1 and 3 days. Twenty μL of MTT solution prepared in PBS (5 mg/mL) was added to each well and incubated at 37 °C for 4 h after the cells were harvested on the

https://doi.org/10.1021/acsomega.4c09945
ACS Omega 2025, 10, 3067−3079

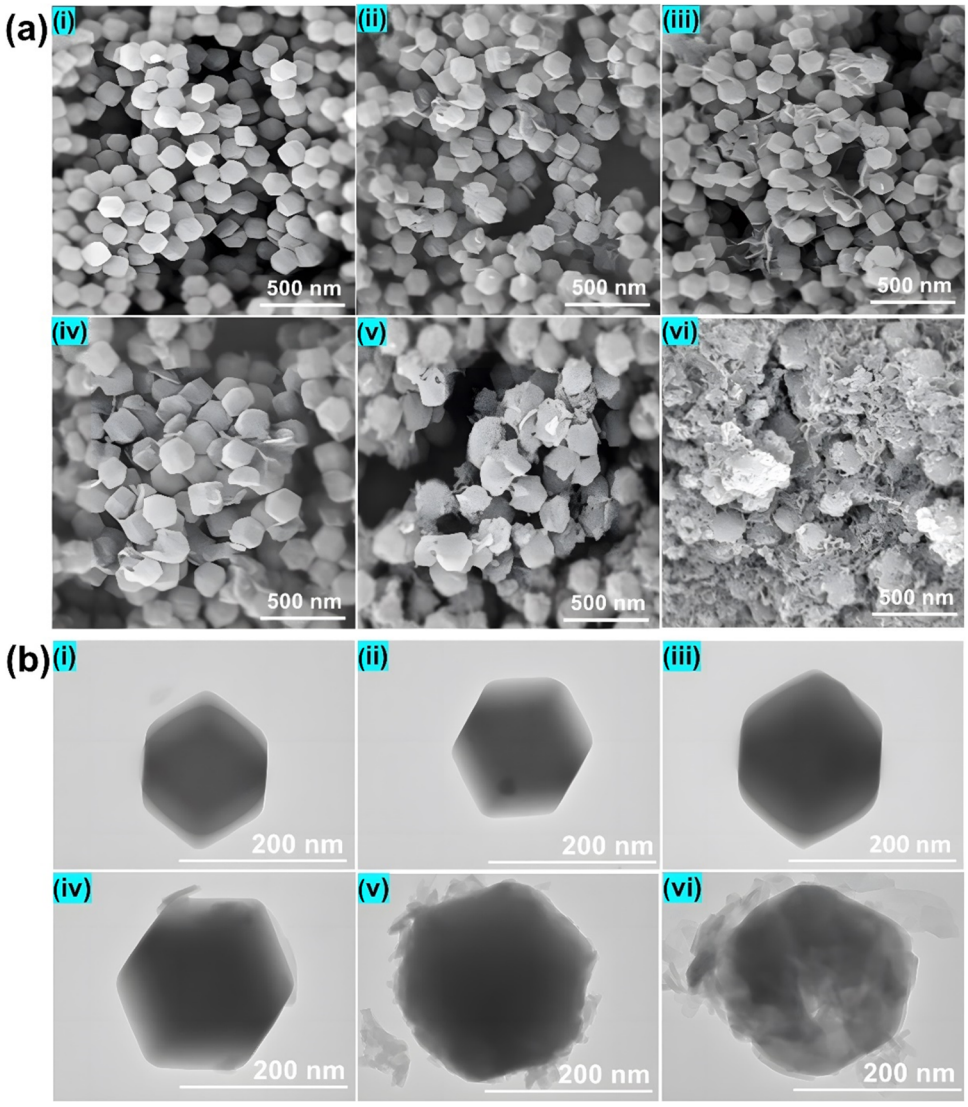

Figure 1. Microscopic morphology observation of ZIF-8 and cur@ZIF-8 (a) SEM and (b) TEM images. (i), (ii), (iii), (iv), (v), and (vi) represent pure ZIF-8, 0.1, 0.3, 0.5, 1, and 2 mg/mL cur loaded ZIF-8, respectively.

first and third days. The MTT solution was used to precipitate the purple formazan crystal. Subsequently, the medium on the cells was removed, and 100 μL of DMSO was added to each well to dissolve the formazan crystal. The mixture was then agitated under dark conditions for 30 min. The absorbance of each well was determined at 490 nm using a microplate spectrophotometer (Tecan M200 Pro, Switzerland).

2.3.10. Antibacterial Test. The antimicrobial activities of cur, ZIF-8, and cur@ZIF-8 were assessed by using gram-negative *Escherichia coli* (ATCC 29522) and gram-positive *Staphylococcus aureus* (ATCC 6538). Both bacterial strains were cultured in liquid nutrient broth at 37 °C for 24 h and then diluted to the desired optical density. For each test, 0.075 ± 0.005 g of the nanoparticles were sterilized for 2 h under exposure to UV light. The sterilized samples were mixed with 500 μL of the diluted culture media and 7 mL of PBS in sterile tubes, which were then shaken for 24 h at 37 °C in an incubator. After incubation, 1 mL of each sample solution was plated onto Petri dishes, nutrient agar was added, and the dishes were incubated overnight. Photographs of the bacterial colonies were taken the following day, and the inhibition rate was calculated by using eq 10.

$$\text{inhibition rate (\%)} = \frac{\text{no. of bacteria in control} - \text{no. of bacteria in sample}}{\text{no. of bacteria in control}} \times 100 \quad (10)$$

2.4. Statistical Analysis. The mean value with ± standard deviation (SD) was used to represent quantitative data. Furthermore, a minimum of three parallel samples were selected for each group. An analysis of variance (ANOVA) with the Scheffé posthoc test was implemented to conduct statistical analysis. A statistically significant disparity between the two groups is present when the p-value is less than 0.05.

3. RESULTS AND DISCUSSION

3.1. Microscopic Morphology Observation. The morphological analysis of ZIF-8 and various concentrations (0.1, 0.3, 0.5, 1, and 2 mg/mL) of cur@ZIF-8 involved a comprehensive examination of nanoparticle characteristics including shape, size, and distribution. Scanning electron microscopy (SEM) characterized the morphologies and sizes of various concentrations (0.1, 0.3, 0.5, 1, and 2 mg/mL) of

https://doi.org/10.1021/acsomega.4c09945
ACS Omega 2025, 10, 3067−3079

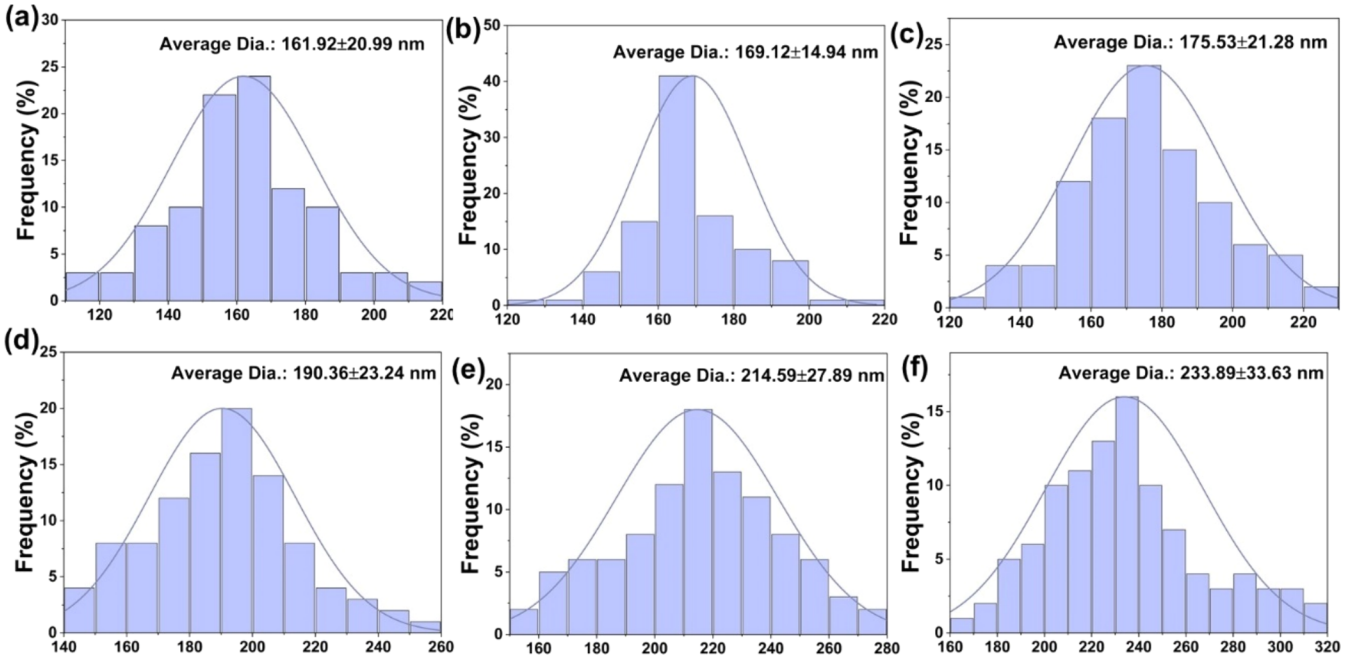

Figure 2. Nanoparticle size distribution. (a–f) Represent pure ZIF-8, 0.1, 0.3, 0.5, 1, and 2 mg/mL cur loaded ZIF-8, respectively.

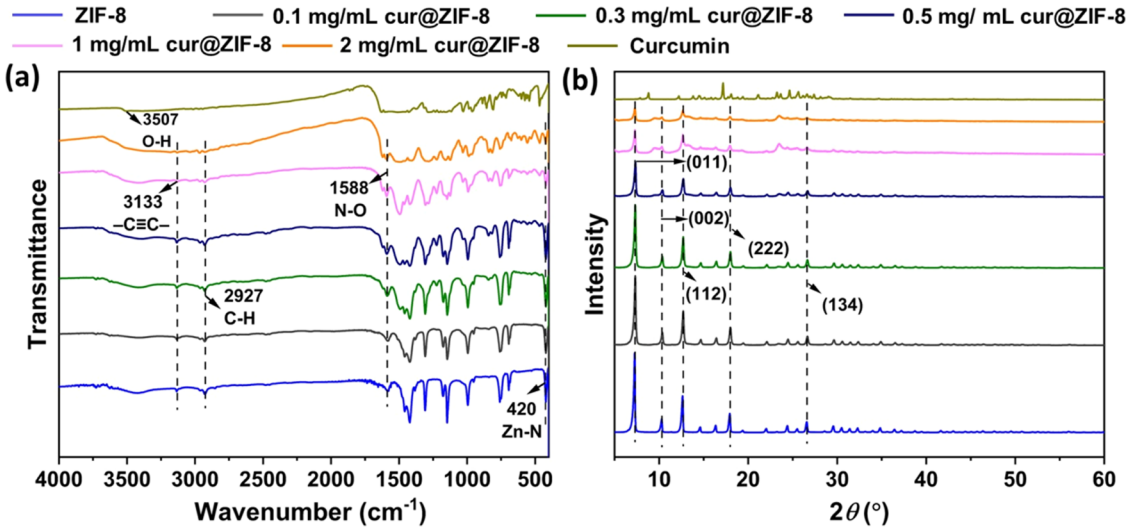

Figure 3. (a) FTIR spectra and (b) XRD spectra of ZIF-8, cur-loaded ZIF-8, and cur.

cur@ZIF-8 and pristine ZIF-8. As depicted in Figure 1a, ZIF-8 and cur@ZIF-8 NPs exhibited uniform rhombic dodecahedral shapes at cur concentrations of 0, 0.1, 0.3, and 0.5 mg/mL. However, notable morphological changes were observed with higher cur concentrations in ZIF-8. At 1 mg/mL, a moderate deformation in the ZIF-8 structure was evident, and at 2 mg/mL, a significant deformation occurred. The excessive curcumin loading disrupts the ZIF-8 structure potentially through curcumin-induced alterations in the coordination environment or the collapse of the framework. Concentration-dependent nanoparticle deformation underscores the importance of optimizing the curcumin loading for nanoparticle stability.

The morphological structures of ZIF-8 and cur@ZIF-8 were observed by using a transmission electron microscope (TEM), as shown in Figure 1b. ZIF-8 and cur@ZIF-8 exhibited the same structures and sizes, which is consistent with the results observed by SEM.

The diameter of the ZIF-8 particles was around 161.92 ± 20.99 nm. However, the size of the nanoparticles became larger when cur was loaded into the ZIF-8 synthesis (see Figure 2). The diameters of 0.1, 0.3, 0.5, 1, and 2 mg/mL cur-loaded ZIF-8 were 169.12 ± 14.94, 175.53 ± 21.28, 190.36 ± 23.24, 214.59 ± 27.89, and 233.89 ± 33.63 nm, respectively, indicating an increase in nanoparticle size after cur loading, consistent with literature reports.[60] The size of cur@ZIF-8 increased as cur increased, which may be explained by the intermolecular hydrogen bond that forms between the phenolic hydroxyl group in cur and the nitrogen atom in 2MIM. Large particles larger than 200 nm are not suitable for carrying drugs.

3.2. FTIR and XRD Spectroscopy Analysis of Cur@ZIF-8.

Figure 3a presents the FTIR spectra of ZIF-8, cur@ZIF-8,

https://doi.org/10.1021/acsomega.4c09945
ACS Omega 2025, 10, 3067−3079

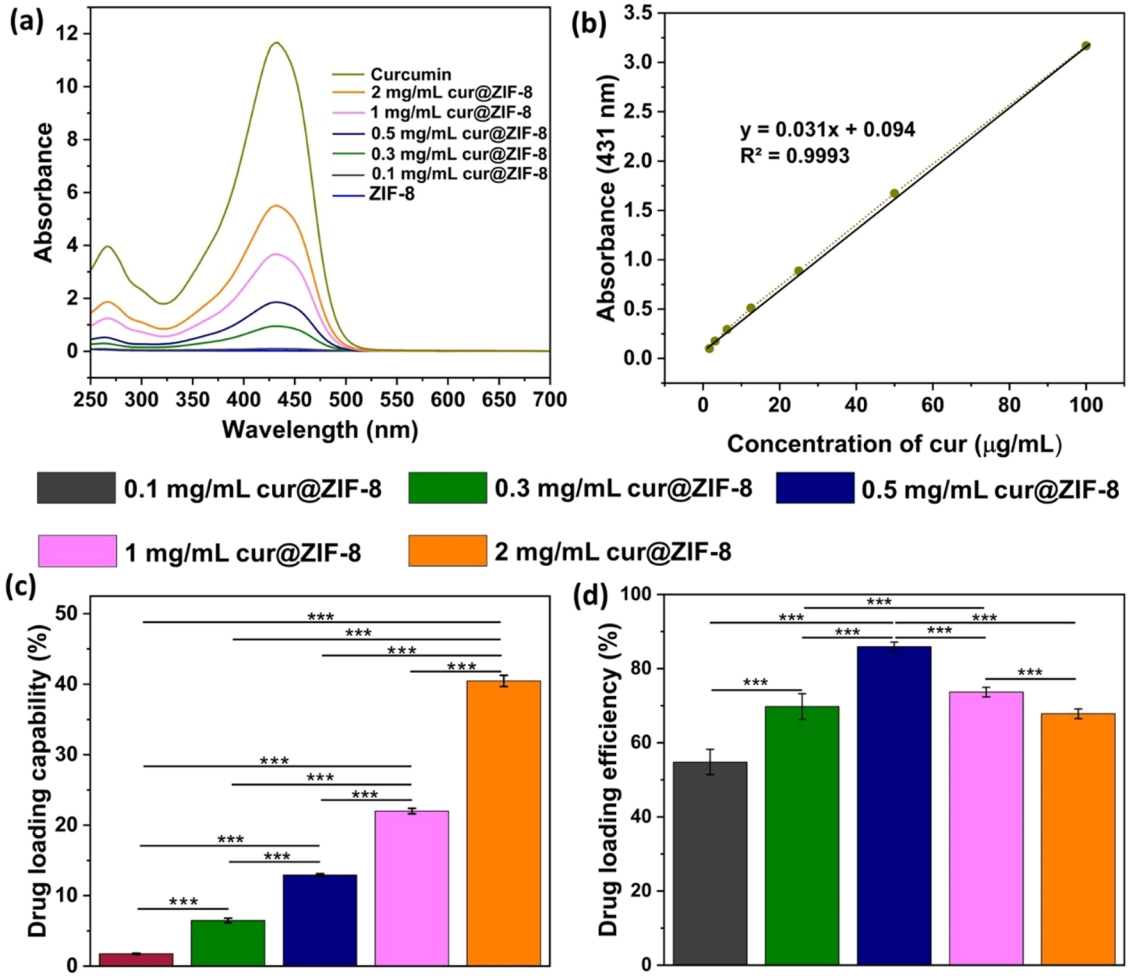

Figure 4. (a) UV spectroscopy curve of ZIF-8, cur@ZIF-8, and curcumin, (b) standard curve of curcumin, (c) drug loading capacity (DLC), and (d) drug loading efficiency (DLE). The data is expressed as the mean value with ± SD, $n = 3$, and $^{***}p < 0.001$.

and cur. ZIF-8 absorption bands at 3133 and 2927 cm^{-1} correspond to C−H stretching of −C≡C− and $-CH_3$, respectively. The bands at 1588 cm^{-1} were ascribed to N−O asymmetric stretching of the nitro compounds, whereas the sharp band at 420 cm^{-1} was designated for N−Zn stretching. ZIF-8 peak position in this investigation aligns well with prior reports.[61−63] The identical peak position was seen at various concentrations (0.1, 0.3, 0.5, 1, and 2 mg/mL) of cur@ZIF-8, indicating that the cur did not alter ZIF-8's chemical structure. Cur displays an O−H stretching vibration peak at 3507 cm^{-1}. However, the O−H peak is absent in cur@ZIF-8, primarily because cur is predominantly encapsulated within the ZIF-8 framework rather than residing on the surface.

The crystallization characteristics of ZIF-8, cur@ZIF-8, and cur are delineated by distinct peaks in their X-ray diffraction (XRD) pattern at particular angles (see Figure 3b). The peaks are identified at 2θ = 7.2, 10.4, 12.6, 17.9, and 26.7° for ZIF-8, corresponding to the planes (011), (002), (112), (222), and (134) accordingly, consistent with the literature.[64] The peak intensity occurs at 2θ = 7.2°, signifying that ZIF-8 exhibits substantial crystallinity. Cur@ZIF-8 exhibited analogous crystalline diffraction peaks in XRD pattern analysis, suggesting that cur did not influence the ZIF-8 crystal structure. However, as the concentration of cur in cur@ZIF-8 increased, the peak intensity diminished.

3.3. UV Spectroscopy, DLC, and DLE. To further confirm that cur is loaded into the ZIF-8 framework, the UV−vis absorption curves of cur, ZIF-8, and cur@ZIF-8 in methanol solution were tested in the wavelength range of 250−800 nm to observe the characteristic absorption bands of the samples, as shown in Figure 4a. Cur shows a characteristic peak at 431 nm; no corresponding characteristic peak is observed for ZIF-8 at around 431 nm. However, cur@ZIF-8 shows a characteristic peak at 427−431 nm, which is due to the loading of cur onto ZIF-8, indicating that cur is successfully loaded onto ZIF-8. Using the characteristic of ZIF-8 decomposing under acidic conditions, we fully dissolved cur@ZIF-8 in an HCl/ethanol solution. The DLC and DLE were calculated using the standard curve of cur in acidic solution. Figure 4b shows the standard curve of cur and the obtained equation from the standard curve.

The DLC (%) for 0.1, 0.3, 0.5, 1, and 2 mg/mL of cur@ZIF-8 were measured 1.73 ± 0.11, 6.49 ± 0.32, 12.93 ± 0.19, 22.01 ± 0.39, 40.47 ± 0.79 (%), respectively (see Figure 4c). The data indicates a progressive rise in DLC (%) with an increasing cur concentration. Initial increments were rapid, but beyond a cur concentration of 1 mg/mL, a gradual increase was observed. Conversely, DLE (%) exhibited an upward trend with increasing cur concentration, reaching its peak (85.91 ± 1.26%) at 0.5 mg/mL cur@ZIF-8 (see Figure 4d). Beyond this concentration, DLE declines, likely due to saturation effects

https://doi.org/10.1021/acsomega.4c09945
ACS Omega 2025, 10, 3067−3079

and limited encapsulation capacity, resulting in less efficient cur uptake. These trends indicate that while ZIF-8 can sustain considerable cur loading, it is most efficient up to a certain threshold, making 0.5 mg/mL a potentially optimal concentration for maximum DLE in cur@ZIF-8 formulations.

3.4. Surface Area and Pore Structure Analysis. The BET analysis determined the surface area and pore structure parameters of ZIF-8 and cur-loaded ZIF-8 at various cur concentrations shown in Table 2 and Figure 5. The BET surface area of pristine ZIF-8 was 1753.45 m^2/g, whereas a progressive decline in surface area with the increase of cur loading of ZIF-8 was observed. The BET surface area was found to be 1703.88 1686.20, 1591.03, 757.07, and 282.98 m^2/g for 0.1, 0.3, 0.5, 1, and 2 mg/mL cur@ZIF-8, respectively (see Table 2). This trend indicates a minor initial decline in surface area (9.26% for 0.5 mg/mL cur@ZIF-8) compared to pure ZIF-8, followed by a more substantial reduction at higher cur concentrations, reaching 56.82 and 83.86% decreases for 1 and 2 mg/mL cur@ZIF-8, respectively. Similar trends were observed in the density functional theory (DFT) surface area and micropore volumes, with notable declines at higher cur concentrations.

Table 2. BET Surface Area and Micropore Volume of ZIF-8 and Cur@ZIF-8

sample	BET surface area (g/m^2)	DFT surface area (g/m^2)	micropore surface area (g/m^2)	micropore volume (cm^3/g)
ZIF-8	1753.45	1023.09	1694.51	0.608
0.1 mg cur@ZIF-8	1703.88	996.91	1653.13	0.594
0.3 mg cur@ZIF-8	1686.20	993.16	1621.65	0.584
0.5 mg cur@ZIF-8	1591.02	916.24	1502.87	0.540
1 mg cur@ZIF-8	757.07	466.99	642.52	0.238
2 mg cur@ZIF-8	282.98	195.32	181.26	0.074

The decline tendency was also observed for the micropore volume. Initial declines were less with a micropore volume decrease of 9.70% for 0.5 mg/mL cur@ZIF-8 concerning pristine ZIF-8. Rapid decreases of micropore volume for 1 and 2 mg of cur-loaded ZIF-8 were observed, 60.85 and 87.82%, respectively. These results suggest that the encapsulation of cur within the ZIF-8 framework effectively reduces the available surface area and micropore volume, especially over 0.5 mg/mL cur encapsulation, due to the physical filling or partial obstruction of the ZIF-8 pores by cur molecules.

The DFT pore size distribution analysis of ZIF-8 and cur@ZIF-8 reveals distinct differences in their pore characteristics following cur encapsulation (see Figure 5a). The pristine ZIF-8, 0.1, 0.3, and 0.5 mg/mL cur@ZIF-8 exhibited a narrow pore size distribution primarily centered in the microporous range, with a predominant peak around 1.2 nm, characteristic of its well-defined microporous framework structure. For more loading of cur, such as 1 and 2 mg/mL cur@ZIF-8, the DFT analysis showed a decrease in the intensity of the peak at 1.2 nm and the emergence of new peaks in the range of (1.5−2) nm, suggesting the formation of larger pores due to the aggregation of cur within the ZIF-8 framework. This shift reflects a reduction in the proportion of accessible micropores and is consistent with the observed decreases in BET surface area and micropore volume. Furthermore, the nitrogen adsorption−desorption isotherms for pure ZIF-8 and cur@ZIF-8 samples displayed Type I profiles (see Figure 5b), with high nitrogen uptake at low relative pressures ($P/P_0 < 0.1$), indicative of microporosity. However, at higher cur concentrations (1 and 2 mg/mL), nitrogen adsorption decreased significantly and a pronounced hysteresis loop appeared, signaling pore deformation due to curcumin loading. These findings collectively suggest that high curcumin loading within ZIF-8 impedes the original microporous structure, altering the material's accessibility and adsorption capacity.

From the above result and discussion, it is observed that 0.5 mg/mL cur@ZIF-8 showed better DLC (%) and highest DLE (%), better BET surface area, and micropore volume without a significant change of ZIF-8 properties in size, shape, and chemical properties. However, further incorporation of cur (such as 1 and 2 mg/mL) results in a highly significant change in ZIF-8 properties. Further, we tested only ZIF-8, cur, and 0.5 mg/mL cur@ZIF-8.

3.5. Thermogravimetric Analysis. The thermal stability of cur, 0.5 mg/mL cur@ZIF-8, and ZIF-8 was assessed using

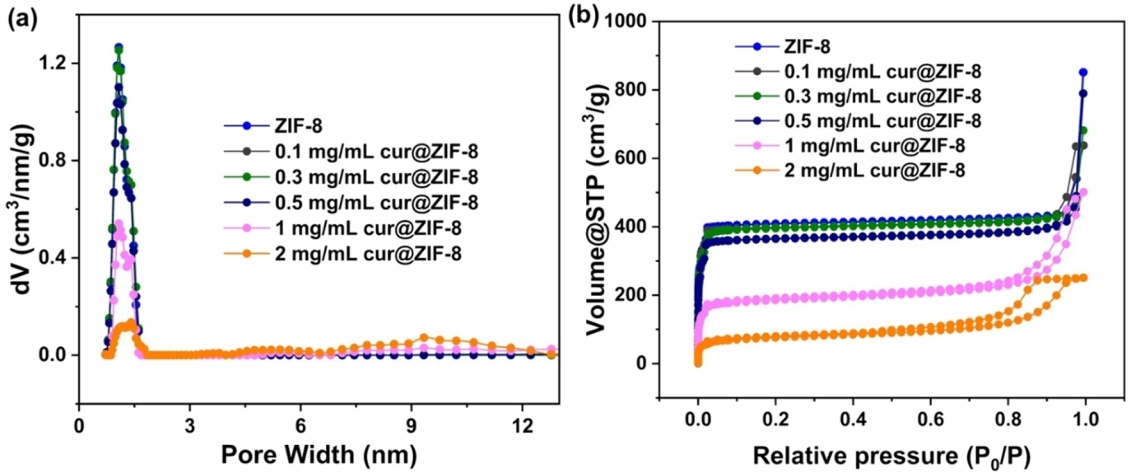

Figure 5. (a) DFT pore size distributions and (b) nitrogen adsorption−desorption isotherms of ZIF-8 and 0.1, 0.3, 0.5, 1, and 2 mg/mL of cur@ZIF-8.

https://doi.org/10.1021/acsomega.4c09945
ACS Omega 2025, 10, 3067−3079

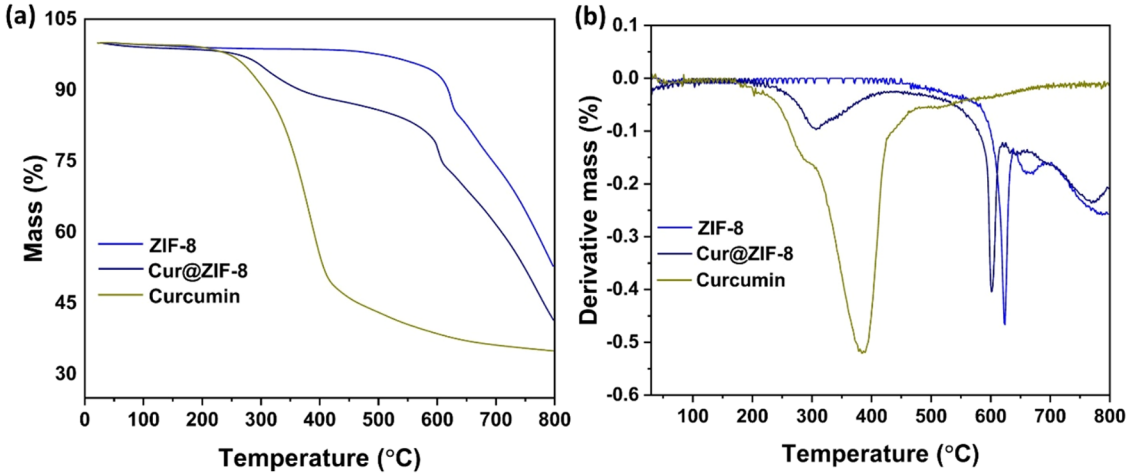

Figure 6. (a) TGA and (b) DTG spectra of ZIF-8, cur-loaded ZIF-8, and cur.

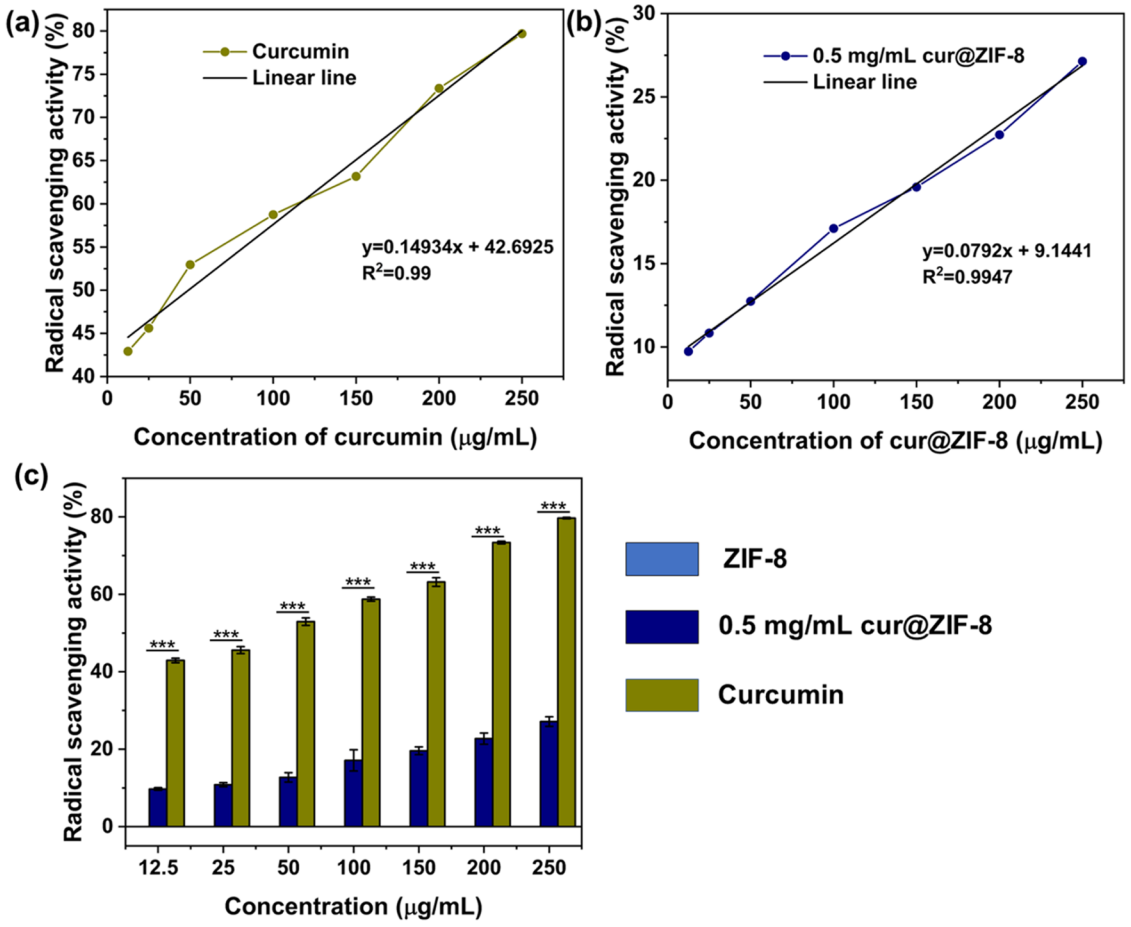

Figure 7. DPPH RSA (%) assessment with regression equation of (a) cur, (b) 0.5 mg/mL cur@ZIF-8, and (c) comparison of RSA (%) between cur and cur@ZIF-8. The data is expressed as the mean value with ± SD, $n = 3$, and $^{***}p < 0.001$.

thermogravimetric analysis (TGA) and differential thermogravimetric analysis (DTG), as depicted in Figure 6a,b, respectively. ZIF-8 demonstrated a singular thermal decomposition phase with a peak decomposition temperature of 623.9 °C and a mass loss rate of 47.16%. Cur exhibited a singular thermal decomposition phase, characterized by a peak decomposition temperature of 383.8 °C and a mass loss rate of 65.06%. Conversely, 0.5 mg/mL cur@ZIF-8 exhibited two separate thermal breakdown phases associated with the cur component and the ZIF-8 component. The maximal decomposition temperatures for these stages were 385.8 and 601.3 °C, respectively. Cur@ZIF-8 mass loss rate was determined to be 48.42%. The integration of cur into ZIF-8 markedly elevated the first thermal decomposition temperature relative to that of free cur. Cur@ZIF-8 demonstrated a weight reduction of 12% relative to that of ZIF-8. The increased weight loss is associated with the curcumin loading capacity

https://doi.org/10.1021/acsomega.4c09945
ACS Omega 2025, 10, 3067−3079

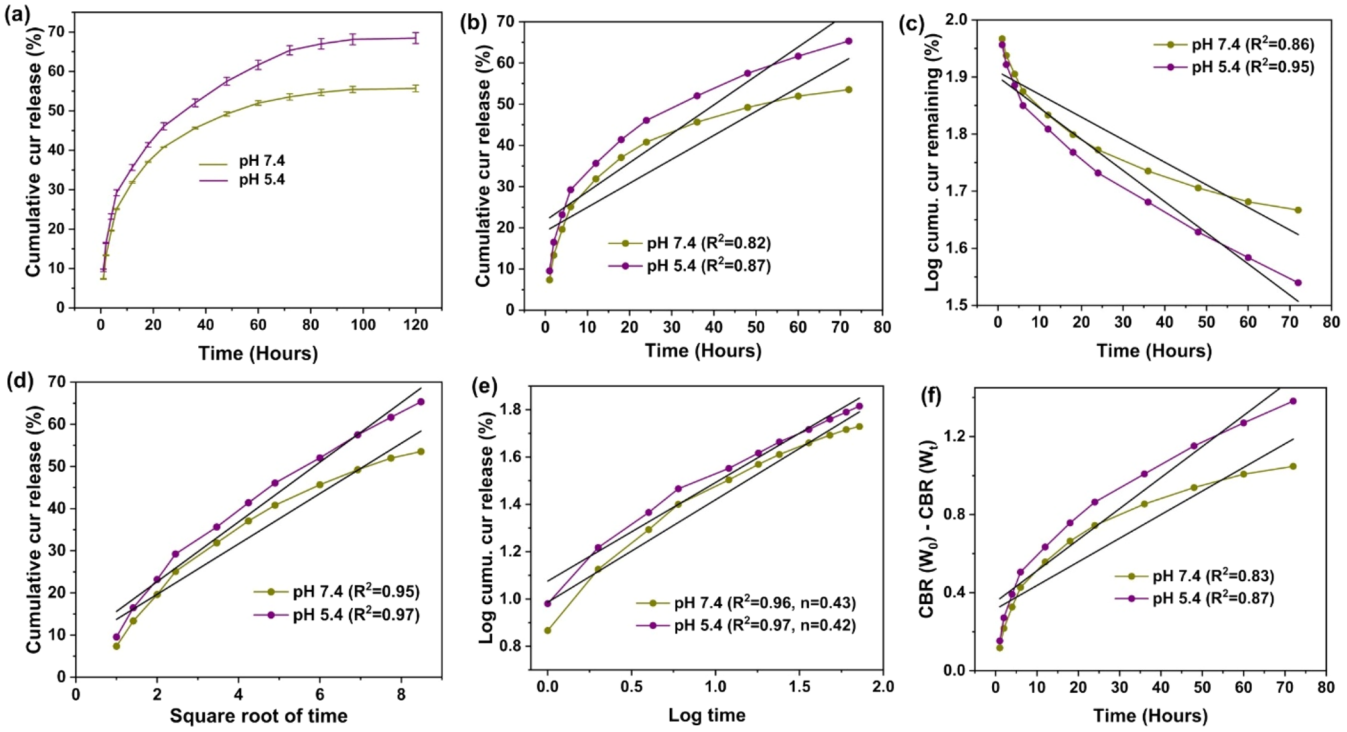

Figure 8. (a) Cumulative cur release profile, (b) zero-order, (c) first-order, (d) Higuchi, (e) Krosmeyer−Peppas, and (f) Hixson−Crowell drug release kinetics model.

(%) in ZIF-8, indicating the effective integration and stability improvement of curcumin within the ZIF-8 framework.

3.6. Antioxidant Property. Antioxidants are critical in maintaining health and preventing disease by neutralizing free radicals. Figure 7a,b illustrates the antioxidant properties (DPPH RSA%) with the regression equation of cur and cur@ZIF-8, respectively. Furthermore, the comparison of RSA (%) between cur and cur@ZIF-8 is shown in Figure 7c. ZIF-8 exhibited no antioxidant activity, whereas cur@ZIF-8 demonstrated moderate antioxidant properties. Cur, on the other hand, showed excellent antioxidant activity. The RSA (%) increased with higher concentrations of cur and cur@ZIF-8. Cur exhibits excellent antioxidant properties due to its chemical structure, including multiple phenolic and methoxy groups.[65] These phenolic groups can donate hydrogen atoms to free radicals, neutralizing them and preventing oxidative damage. Moreover, cur's structure allows it to stabilize free radicals by delocalizing their unpaired electrons, further enhancing its antioxidant efficacy. The presence of conjugated double bonds in cur also contributes to its ability to scavenge free radicals efficiently.[66]

The term IC_{50} refers to the inhibitory concentration at 50%, which represents half of the maximum inhibitory concentration of a compound. The utilization of the IC_{50} value is important, as it precisely measures the amount of a drug required to inhibit a biological process by 50%. The IC_{50} value of cur was found to be 48.93 μg/mL, almost the same finding as previous literature,[67] whereas the IC_{50} value for cur@ZIF-8 was determined to be 515.86 μg/mL, which is approximately 11 times higher than that of cur alone. ZIF-8 alone did not exhibit any antioxidant properties; cur is the primary reason for the antioxidant properties observed in cur@ZIF-8. This IC_{50} value also demonstrates the successful incorporation of cur into cur@ZIF-8.

3.7. Drug Release Profile and Kinetics Analysis. The pH level of the local microenvironment is a crucial element that can have both direct and indirect effects on repair responses during the wound-healing process.[68] The pH of normal skin ranges from 4.8 to 6.0 due to the organic acid released by keratinocytes.[69] Drug release assays were conducted in vitro using phosphate buffer solution (PBS) (pH 7.4 and 5.4) to examine its controlled release characteristics. Figure 8a illustrates the drug release of cur@ZIF-8 in PBS at pH levels of 5.4 and 7.4.

The results indicate that the drug release rate of cur@ZIF-8 was faster in acidic (pH 5.4) conditions compared to that in neutral (pH 7.4). At all-time points, the cumulative drug release rate in the acidic environment was higher than that in the neutral environment, demonstrating significant acid-responsive characteristics. This behavior is attributed to the breakdown of ZIF-8 under acidic conditions, which is a known pH-responsive property. At 24 h and 5 days, the cumulative drug release rate at pH 5.4 was 48.08 and 68.47%, respectively, which was almost 8 and 13% higher than at pH 7.4 at the same time interval. The pH-responsive release property of ZIF-8 can reduce premature drug release during blood circulation while particularly increasing drug release in acidic wound microenvironments. This characteristic will undoubtedly be advantageous for wound healing in vivo.

The release kinetics of cur from 0.5 mg/mL cur@ZIF-8 were analyzed using several mathematical models, including zero-order, first-order, Higuchi, K−P, and H−C (see Figure 8b−f). For pH 7.4 and pH 5.4, the K−P model showed the highest correlation coefficient (R^2) of 0.96 and 0.97, respectively, so the K−P model fitted the release profile of cur the best. The release exponent (n) in the K−P model, where n is less than 0.5 for both pH 7.4 and pH 5.4, indicates quasi-Fickian diffusion.[70] This suggests that curcumin release occurs partially

https://doi.org/10.1021/acsomega.4c09945
ACS Omega 2025, 10, 3067−3079

through diffusion, governed by both diffusion and structural constraints of the ZIF-8 matrix.

3.8. Cell Proliferation. Cellular biocompatibility assessments of ZIF-8, cur@ZIF-8, and cur were conducted using the standard MTT assay on HDF cells. The MTT can be converted into water-insoluble blue-violet crystals by succinate dehydrogenase, which is present exclusively in the mitochondria of viable cells, excluding nonviable cells. Subsequent semiquantitative MTT assay demonstrated that numerous cells remained viable in the control group devoid of any samples (see Figure 9).

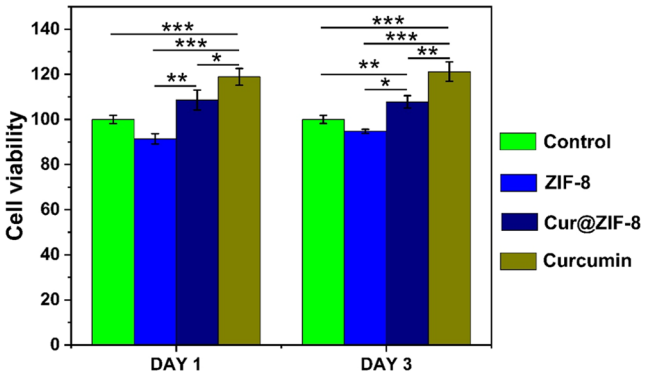

Figure 9. OD value of cell culture at day 1, and day 3 of control, ZIF-8, cur@ZIF-8, and cur. The data is expressed as the mean value with ± SD, $n = 3$, $^{*}p < 0.05$, $^{**}p < 0.01$ and $^{***}p < 0.001$.

The cell viability of cur and cur@ZIF-8 exceeded that of the control group. Pure ZIF-8 exhibits cytotoxicity toward human dermal fibroblast (HDF) cells. The semiquantitative analysis indicated that cur exhibited the highest cell viability value, whereas cur@ZIF-8 was somewhat inferior without a significant difference; nonetheless, pure ZIF-8 demonstrated considerable cytotoxicity. The results suggested that HDF cells may attach to and survive on cur@ZIF-8; nevertheless, ZIF-8 could harm certain living cells. Previous studies have demonstrated that excessive ZIF-8 can dramatically enhance cytotoxicity.[71,72]

3.9. Antibacterial Activity. The antibacterial efficacy of ZIF-8, cur@ZIF-8, and cur was assessed against *E. coli* and *S. aureus* and is shown in Figure 10a,b.

The antibacterial action of ZIF-8 can be linked to the presence of zinc ions (Zn^{2+}), which ZIF-8 undoubtedly showed antibacterial activity, and the inhibition rate against *E. coli* and *S. aureus* reached 99 and 99%, respectively. Cur without further treatment showed less antibacterial efficacy, and the inhibition rate of cur against *E. coli* and *S. aureus* was found to be 40.02 ± 2.77 and 24.56 ± 1.87%, respectively. However, the antibacterial efficacy of cur is significantly enhanced by encapsulating it in ZIF-8. The inhibition rates of cur@ZIF-8 against *E. coli* and *S. aureus* reached 99 and 99%, respectively. Changmai et al.[73] have demonstrated that ZIF-8 containing cur has enhanced antibacterial properties in comparison to cur alone, suggesting that this composite has the potential to fight bacterial infections effectively. The synergistic antibacterial activity can also be described as the distinctive characteristics of ZIF-8, including its stability, extensive surface area, and controlled release capabilities.

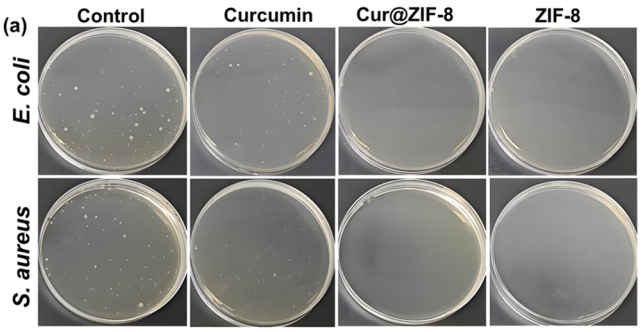

(b)

Samples	Rate of Inhibition (%)	
	E. coli	*S. aureus*
Control	/	/
Curcumin	40.02±2.77	24.56±1.87
Cur@ZIF-8	> 99	> 99
ZIF-8	> 99	> 99

Figure 10. Antibacterial activity (a) digital of image of *E. coli* and *S. aureus* bacteria growth on Petri dish, and (b) Inhibition rates against *E. coli* and *S. aureus* after culture for 24 h against cur, cur@ZIF-8 and ZIF-8.

4. CONCLUSIONS

This investigation of the potential for biomedical applications of cur-loaded zeolitic imidazolate framework-8 nanoparticles (cur@ZIF-8) has yielded valuable insights. Throughout synthesis and characterization using SEM, TEM, XRD, and FTIR, it confirmed the successful encapsulation of cur within ZIF-8 while preserving its structural integrity. 0.5 mg/mL cur@ZIF-8 possesses higher DLE (85.91 ± 1.26%), DLC (12.93 ± 0.119%), better BET surface area (1591.02 m^2/g), and micropore volume (0.540 cm^3/g), excellent biocompatibility, and high stability at physiological conditions, which are ideal candidate carriers for drug delivery. Furthermore, the study of drug release kinetics elucidated the controlled release behavior of cur from ZIF-8, indicating its potential for sustained therapeutic effects. Biomedical evaluations, including MTT assay for cell proliferation assessment, revealed the biocompatibility of cur@ZIF-8 NPs, paving the way for their application in drug delivery and wound healing. Moreover, these findings demonstrated the cur@ZIF-8 NPs promising antibacterial and antioxidant properties, showcasing their versatility for antibacterial infections and oxidative stress. By harnessing the potential of cur@ZIF-8 NPs, we can advance drug delivery systems and contribute to the development of innovative biomedical interventions with significant clinical impact.

AUTHOR INFORMATION

Corresponding Authors

Shaojuan Chen − *State Key Laboratory of Bio-Fibers and Eco-Textiles, College of Textiles and Clothing, Qingdao University, Qingdao 266071, China*; Email: qdchshj@126.com

Shaohua Wu − *State Key Laboratory of Bio-Fibers and Eco-Textiles, College of Textiles and Clothing, Qingdao University, Qingdao 266071, China*; orcid.org/0000-0002-7099-857X; Email: shaohua.wu@qdu.edu.cn

Authors

Mahbubur Rahman − *State Key Laboratory of Bio-Fibers and Eco-Textiles, College of Textiles and Clothing, Qingdao*

https://doi.org/10.1021/acsomega.4c09945
ACS Omega 2025, 10, 3067−3079

University, Qingdao 266071, China; Department of Textile Engineering, Mawlana Bhashani Science and Technology University, Tangail 1902, Bangladesh

Mohashin Kabir − *State Key Laboratory of Bio-Fibers and Eco-Textiles, College of Textiles and Clothing, Qingdao University, Qingdao 266071, China; Department of Textile Engineering, Mawlana Bhashani Science and Technology University, Tangail 1902, Bangladesh;* orcid.org/0009-0003-9722-1300

Tarikul Islam − *Department of Textiles, Merchandising, and Interiors, University of Georgia, Athens, Georgia 30602, United States; Department of Textile Engineering, Jashore University of Science and Technology, Jashore 7408, Bangladesh;* orcid.org/0000-0002-3106-378X

Yafei Wang − *State Key Laboratory of Bio-Fibers and Eco-Textiles, College of Textiles and Clothing, Qingdao University, Qingdao 266071, China*

Qi Meng − *State Key Laboratory of Bio-Fibers and Eco-Textiles, College of Textiles and Clothing, Qingdao University, Qingdao 266071, China*

Hailei Liu − *State Key Laboratory of Bio-Fibers and Eco-Textiles, College of Textiles and Clothing, Qingdao University, Qingdao 266071, China*

Complete contact information is available at: https://pubs.acs.org/10.1021/acsomega.4c09945

Author Contributions

Conceptualization, M.R., S.C., and S.W.; methodology, M.R., M.K., Y.W., S.C., and S.W.; formal analysis, M.R., M.K., T.I., and H.L.; investigation, M.R., Y.Q., Q.M., and H.L.; validation, M.R., M.K., and T.I.; resources, S.C. and S.W.; visualization, M.R., T.I., Y.W., Q.M., and H.L.; supervision, S.C., and S.W.; funding acquisition, S.C., and S.W.; project administration, S.C., and S.W.; original draft, M.R.; writing, review, and editing, M.R., M.K., T.I., S.C., and S.W.; and all authors contributed to the article and approved the submitted version.

Notes

The authors declare no competing financial interest.

■ ACKNOWLEDGMENTS

The authors thank the State Key Laboratory of Bio-Fibers and Eco-Textiles at Qingdao University, Qingdao, China, for financial support under grant number TSKT202102.

■ REFERENCES

(1) Joseph, X.; Akhil, V.; Arathi, A.; Mohanan, P. V. Nano-biomaterials in support of drug delivery related issues. *Mater. Sci. Eng., B* **2022**, *279*, No. 115680.

(2) El-Saadony, M. T.; Yang, T.; Korma, S. A.; Sitohy, M.; Abd El-Mageed, T. A.; Selim, S.; Al Jaouni, S. K.; Salem, H. M.; Mahmmod, Y.; Soliman, S. M.; et al. Impacts of turmeric and its principal bioactive curcumin on human health: Pharmaceutical, medicinal, and food applications: A comprehensive review. *Front. Nutr.* **2023**, *9*, No. 1040259.

(3) Hassan, S. F.; Asghar, S.; Ullah Khan, I.; Munir, R.; Khalid, S. H. Curcumin Encapsulation in Geranium Oil Microemulsion Elevates Its Antibacterial, Antioxidant, Anti-Inflammatory, and Anticancer Activities. *ACS Omega* **2024**, *9* (5), 5624−5636.

(4) Li, Z.; Shi, M.; Li, N.; Xu, R. Application of functional biocompatible nanomaterials to improve curcumin bioavailability. *Front. Chem.* **2020**, *8*, No. 589957.

(5) Madamsetty, V. S.; Vazifehdoost, M.; Alhashemi, S. H.; Davoudi, H.; Zarrabi, A.; Dehshahri, A.; Fekri, H. S.; Mohammadinejad, R.; Thakur, V. K. Next-generation hydrogels as biomaterials for biomedical applications: exploring the role of curcumin. *ACS Omega* **2023**, *8* (10), 8960−8976.

(6) Szegedi, A.; Shestakova, P.; Trendafilova, I.; Mihayi, J.; Tsacheva, I.; Mitova, V.; Kyulavska, M.; Koseva, N.; Momekova, D.; Konstantinov, S.; et al. Modified mesoporous silica nanoparticles coated by polymer complex as novel curcumin delivery carriers. *J. Drug Delivery Sci. Technol.* **2019**, *49*, 700−712.

(7) Elbialy, N. S.; Aboushoushah, S. F.; Sofi, B. F.; Noorwali, A. Multifunctional curcumin-loaded mesoporous silica nanoparticles for cancer chemoprevention and therapy. *Microporous Mesoporous Mater.* **2020**, *291*, No. 109540.

(8) Song, Y.; Cai, L.; Tian, Z.; Wu, Y.; Chen, J. Phytochemical curcumin-coformulated, silver-decorated melanin-like polydopamine/mesoporous silica composites with improved antibacterial and chemotherapeutic effects against drug-resistant cancer cells. *ACS Omega* **2020**, *5* (25), 15083−15094.

(9) Mahmoudi, A.; Kesharwani, P.; Majeed, M.; Teng, Y.; Sahebkar, A. Recent advances in nanogold as a promising nanocarrier for curcumin delivery. *Colloids Surf., B* **2022**, *215*, No. 112481.

(10) Sindhu, K.; Rajaram, A.; Sreeram, K.; Rajaram, R. Curcumin conjugated gold nanoparticle synthesis and its biocompatibility. *RSC Adv.* **2014**, *4* (4), 1808−1818.

(11) Garg, S.; Garg, A. Encapsulation of curcumin in silver nanoparticle for enhancement of anticancer drug delivery. *Int. J. Pharm. Sci. Res.* **2018**, *9* (3), 1160−1166.

(12) Braga, T. L.; de Souza Rossin, A. R.; Fernandes, J. A.; de Mendonça, P. D. S. B.; de Castro-Hoshino, L. V.; Baesso, M. L.; de Freitas, C. F.; Radovanovic, E.; Caetano, W. Electrospun silver nanoparticles/curcumin-loaded nanohybrids for Photodynamic Therapy. *Appl. Mater. Today* **2024**, *36*, No. 102073.

(13) Jose, R.; Jothi, N. N.; Jothi, N. The synthesis and characterisation of curcumin loaded Ag (1-X) Ni X Fe2 O4 for drug delivery. *Mater. Technol.* **2021**, *36* (6), 339−346.

(14) Moussa, Z.; Hmadeh, M.; Abiad, M. G.; Dib, O. H.; Patra, D. Encapsulation of curcumin in cyclodextrin-metal organic frameworks: Dissociation of loaded CD-MOFs enhances stability of curcumin. *Food Chem.* **2016**, *212*, 485−494.

(15) Serri, C.; Argirò, M.; Piras, L.; Mita, D. G.; Saija, A.; Mita, L.; Forte, M.; Giarra, S.; Biondi, M.; Crispi, S.; Mayol, L. Nano-precipitated curcumin loaded particles: Effect of carrier size and drug complexation with (2-hydroxypropyl)-β-cyclodextrin on their biological performances. *Int. J. Pharm.* **2017**, *520* (1−2), 21−28.

(16) Gou, M.; Men, K.; Shi, H.; Xiang, M.; Zhang, J.; Song, J.; Long, J.; Wan, Y.; Luo, F.; Zhao, X.; Qian, Z. Curcumin-loaded biodegradable polymeric micelles for colon cancer therapy in vitro and in vivo. *Nanoscale* **2011**, *3* (4), 1558−1567.

(17) Chignell, C. F.; Bilskj, P.; Reszka, K. J.; Motten, A. G.; Sik, R. H.; Dahl, T. A. Spectral and photochemical properties of curcumin. *Photochem. Photobiol.* **1994**, *59* (3), 295−302.

(18) Feng, T.; Wei, Y.; Lee, R. J.; Zhao, L. Liposomal curcumin and its application in cancer. *Int. J. Nanomed.* **2017**, *12*, 6027−6044.

(19) Storka, A.; Vcelar, B.; Klickovic, U.; Gouya, G.; Weisshaar, S.; Aschauer, S.; Bolger, G.; Helson, L.; Woltz, M. Safety, tolerability and pharmacokinetics of liposomal curcumin (Lipocurc) in healthy humans. *Int. J. Clin. Pharmacol. Ther.* **2015**, *53* (1), 54−65.

(20) Xu, Y.-Q.; Chen, W.-R.; Tsosie, J. K.; Xie, X.; Li, P.; Wan, J.-B.; He, C.-W.; Chen, M.-W. Niosome encapsulation of curcumin: characterization and cytotoxic effect on ovarian cancer cells. *J. Nanomater.* **2016**, *2016* (1), No. 6365295.

(21) Tavano, L.; Muzzalupo, R.; Picci, N.; de Cindio, B. Co-encapsulation of antioxidants into niosomal carriers: gastrointestinal release studies for nutraceutical applications. *Colloids Surf., B* **2014**, *114*, 82−88.

(22) Archana, A.; Vijayasri, K.; Madhurim, M.; Kumar, C. Curcumin loaded nano cubosomal hydrogel: preparation, in vitro characterization and antibacterial activity. *Chem. Sci. Trans.* **2015**, *4* (1), 75−80.

(23) Tu, Y. S.; Fu, J.; Sun, D.; Zhang, J.; Yao, N.; Huang, D.; Shi, Z. Preparation, characterisation and evaluation of curcumin with

piperine-loaded cubosome nanoparticles. *J. Microencapsulation* **2014**, *31* (6), 551−559.
(24) Rahman, M.; Kabir, M.; Chen, S.; Wu, S. Developments, applications, and challenges of metal−organic frameworks@textile composites: A state-of-art review. *Eur. Polym. J.* **2023**, *199*, No. 112480.
(25) Zheng, F.; Zhang, Z.; Zhang, C.; Chen, W. Advanced electrocatalysts based on metal−organic frameworks. *ACS Omega* **2020**, *5* (6), 2495−2502.
(26) Zhu, Q.-L.; Xu, Q. Metal−organic framework composites. *Chem. Soc. Rev.* **2014**, *43* (16), 5468−5512.
(27) Cheon, Y. E.; Suh, M. P. Enhanced hydrogen storage by palladium nanoparticles fabricated in a redox-active metal−organic framework. *Angew. Chem.* **2009**, *121* (16), 2943−2947.
(28) Wong-Foy, A. G.; Matzger, A. J.; Yaghi, O. M. Exceptional H2 saturation uptake in microporous metal−organic frameworks. *J. Am. Chem. Soc.* **2006**, *128* (11), 3494−3495.
(29) Ma, L.; Abney, C.; Lin, W. Enantioselective catalysis with homochiral metal−organic frameworks. *Chem. Soc. Rev.* **2009**, *38* (5), 1248−1256.
(30) Chughtai, A. H.; Ahmad, N.; Younus, H. A.; Laypkov, A.; Verpoort, F. Metal−organic frameworks: versatile heterogeneous catalysts for efficient catalytic organic transformations. *Chem. Soc. Rev.* **2015**, *44* (19), 6804−6849.
(31) Dhakshinamoorthy, A.; Garcia, H. Metal−organic frameworks as solid catalysts for the synthesis of nitrogen-containing heterocycles. *Chem. Soc. Rev.* **2014**, *43* (16), 5750−5765.
(32) Zhu, L.; Liu, X.-Q.; Jiang, H.-L.; Sun, L.-B. Metal−organic frameworks for heterogeneous basic catalysis. *Chem. Rev.* **2017**, *117* (12), 8129−8176.
(33) Li, J.-R.; Sculley, J.; Zhou, H.-C. Metal−organic frameworks for separations. *Chem. Rev.* **2012**, *112* (2), 869−932.
(34) Zhang, Z.; Zhao, Y.; Gong, Q.; Li, Z.; Li, J. MOFs for CO2 capture and separation from flue gas mixtures: the effect of multifunctional sites on their adsorption capacity and selectivity. *Chem. Commun.* **2013**, *49* (7), 653−661.
(35) Fang, G.; Zhou, J.; Liang, C.; Pan, A.; Zhang, C.; Tang, Y.; Tan, X.; Liu, J.; Liang, S. MOFs nanosheets derived porous metal oxide-coated three-dimensional substrates for lithium-ion battery applications. *Nano Energy* **2016**, *26*, 57−65.
(36) Bai, Z.; Zhang, Y.; Zhang, Y.; Guo, C.; Tang, B.; Sun, D. MOFs-derived porous Mn2O3 as high-performance anode material for Li-ion battery. *J. Mater. Chem. A* **2015**, *3* (10), 5266−5269.
(37) Liu, S.; Zhou, J.; Song, H. Tailoring Highly N-Doped Carbon Materials from Hexamine-Based MOFs: Superior Performance and New Insight into the Roles of N Configurations in Na-Ion Storage. *Small* **2018**, *14* (12), No. 1703548.
(38) Bétard, A.; Fischer, R. A. Metal−organic framework thin films: from fundamentals to applications. *Chem. Rev.* **2012**, *112* (2), 1055−1083.
(39) Kreno, L. E.; Leong, K.; Farha, O. K.; Allendorf, M.; Van Duyne, R. P.; Hupp, J. T. Metal−organic framework materials as chemical sensors. *Chem. Rev.* **2012**, *112* (2), 1105−1125.
(40) Huxford, R. C.; Della Rocca, J.; Lin, W. Metal−organic frameworks as potential drug carriers. *Curr. Opin. Chem. Biol.* **2010**, *14* (2), 262−268.
(41) Horcajada, P.; Gref, R.; Baati, T.; Allan, P. K.; Maurin, G.; Couvreur, P.; Férey, G.; Morris, R. E.; Serre, C. Metal−organic frameworks in biomedicine. *Chem. Rev.* **2012**, *112* (2), 1232−1268.
(42) Horcajada, P.; Chalati, T.; Serre, C.; Gillet, B.; Sebrie, C.; Baati, T.; Eubank, J. F.; Heurtaux, D.; Clayette, P.; Kreuz, C.; et al. Porous metal−organic-framework nanoscale carriers as a potential platform for drug delivery and imaging. *Nat. Mater.* **2010**, *9* (2), 172−178.
(43) Kundu, T.; Mitra, S.; Patra, P.; Goswami, A.; Díaz Díaz, D.; Banerjee, R. Mechanical Downsizing of a Gadolinium (III)-based Metal−Organic Framework for Anticancer Drug Delivery. *Chem. - Eur. J.* **2014**, *20* (33), 10514−10518.
(44) Rahman, M.; Kabir, M.; Li, K.; Li, Y.; Chen, S.; Wu, S. Electrospun Zeolitic Imidazole Framework-8 Loaded Silk Fibroin/Polycaprolactone Nanofibrous Scaffolds for Biomedical Application. *J. Mech. Behav. Biomed. Mater.* **2024**, *160*, No. 106769.
(45) Vasconcelos, I. B.; da Silva, T. G.; Militão, G. C.; Soares, T. A.; Rodrigues, N. M.; Rodrigues, M. O.; da Costa, N. B.; Freire, R. O.; Junior, S. A. Cytotoxicity and slow release of the anti-cancer drug doxorubicin from ZIF-8. *RSC Adv.* **2012**, *2* (25), 9437−9442.
(46) Yan, J.; Liu, C.; Wu, Q.; Zhou, J.; Xu, X.; Zhang, L.; Wang, D.; Yang, F.; Zhang, H. Mineralization of pH-Sensitive Doxorubicin Prodrug in ZIF-8 to Enable Targeted Delivery to Solid Tumors. *Anal. Chem.* **2020**, *92* (16), 11453−11461.
(47) Zheng, C.; Wang, Y.; Phua, S. Z. F.; Lim, W. Q.; Zhao, Y. ZnO−DOX@ ZIF-8 core−shell nanoparticles for pH-responsive drug delivery. *ACS Biomater. Sci. Eng.* **2017**, *3* (10), 2223−2229.
(48) Mazloum-Ardakani, M.; Shaker-Ardakani, N.; Ebadi, A. Development of Metal−Organic Frameworks (ZIF-8) as Low-Cost Carriers for Sustained Release of Hydrophobic and Hydrophilic Drugs: In Vitro Evaluation of Anti-Breast Cancer and Anti-Infection Effect. *J. Cluster Sci.* **2023**, *34* (4), 1861−1876.
(49) Gomar, M.; Yeganegi, S. Adsorption of 5-fluorouracil, hydroxyurea and mercaptopurine drugs on zeolitic imidazolate frameworks (ZIF-7, ZIF-8 and ZIF-9). *Microporous Mesoporous Mater.* **2017**, *252*, 167−172.
(50) Zhou, Z.; Ke, Q.; Wu, M.; Zhang, L.; Jiang, K. Pore Space Partition Approach of ZIF-8 for pH Responsive Codelivery of Ursolic Acid and 5-Fluorouracil. *ACS Mater. Lett.* **2023**, *5* (2), 466−472.
(51) Gong, J.; Li, X.; Li, S.; Xu, M.; Dai, W. ZIF-8-based core/shell nanocarriers for relieving multidrug resistance in cancer therapy. *New J. Chem.* **2023**, *47* (48), 22495−22507.
(52) Liu, G.; Xu, Y.; Han, Y.; Wu, J.; Xu, J.; Meng, H.; Zhang, X. Immobilization of lysozyme proteins on a hierarchical zeolitic imidazolate framework (ZIF-8). *Dalton Trans.* **2017**, *46* (7), 2114−2121.
(53) Zheng, H.; Sun, T.; Zeng, Y.; Zheng, M.-Y.; Zhang, F.-Z.; Wang, Y.-L.; Lin, Z.-J.; Lin, R.-G. Hierarchical Micro- and Mesoporous Zeolitic Imidazolate Framework-8-Based Enzyme Hybrid for Combination Antimicrobial by Lysozyme and Lactoferrin. *Inorg. Chem.* **2024**, *63* (26), 12377−12384.
(54) Xu, M.; Hu, Y.; Ding, W.; Li, F.; Lin, J.; Wu, M.; Wu, J.; Wen, L.-P.; Qiu, B.; Wei, P.-F.; Li, P. Rationally designed rapamycin-encapsulated ZIF-8 nanosystem for overcoming chemotherapy resistance. *Biomaterials* **2020**, *258*, No. 120308.
(55) Zhang, S.; Li, J.; Yan, L.; You, Y.; Zhao, F.; Cheng, J.; Yang, L.; Sun, Y.; Chang, Q.; Liu, R.; Li, Y. Zeolitic imidazolate framework-8 (ZIF-8) as a drug delivery vehicle for the transport and release of telomerase inhibitor BIBR 1532. *Nanomaterials* **2023**, *13* (11), 1779.
(56) Zheng, M.; Liu, S.; Guan, X.; Xie, Z. One-Step Synthesis of Nanoscale Zeolitic Imidazolate Frameworks with High Curcumin Loading for Treatment of Cervical Cancer. *ACS Appl. Mater. Interfaces* **2015**, *7* (40), 22181−22187.
(57) Cui, C.; Sun, S.; Li, X.; Chen, S.; Wu, S.; Zhou, F.; Ma, J. Optimizing the chitosan-PCL based membranes with random/aligned fiber structure for controlled ciprofloxacin delivery and wound healing. *Int. J. Biol. Macromol.* **2022**, *205*, 500−510.
(58) Brand-Williams, W.; Cuvelier, M. E.; Berset, C. Use of a free radical method to evaluate antioxidant activity. *LWT - Food Sci. Technol.* **1995**, *28* (1), 25−30.
(59) Frankel, E. N.; Meyer, A. S. The problems of using one-dimensional methods to evaluate multifunctional food and biological antioxidants. *J. Sci. Food Agric.* **2000**, *80* (13), 1925−1941.
(60) Yu, S.; Wang, S.; Xie, Z.; Yu, S.; Li, L.; Xiao, H.; Song, Y. Hyaluronic acid coating on the surface of curcumin-loaded ZIF-8 nanoparticles for improved breast cancer therapy: An in vitro and in vivo study. *Colloids Surf., B* **2021**, *203*, No. 111759.
(61) Lee, S.; Lei, Y.; Wang, D.; Li, C.; Cheng, J.; Wang, J.; Meng, W.; Liu, M. The Study of Zeolitic Imidazolate Framework (ZIF-8) Doped Polyvinyl Alcohol/Starch/Methyl Cellulose Blend Film. *Polymers* **2019**, *11* (12), 1986.
(62) Kebria, M. R. S.; Rahimpour, A.; Bakeri, G.; Abedini, R. Experimental and theoretical investigation of thin ZIF-8/chitosan

https://doi.org/10.1021/acsomega.4c09945
ACS Omega 2025, 10, 3067−3079

coated layer on air gap membrane distillation performance of PVDF membrane. *Desalination* **2019**, *450*, 21−32.
(63) Wang, M.; Song, X.; Jiang, J.; Xia, J.; Li, M. Influence of Zeolitic imidazolate framework-8 on the thermal stabilization of poly (vinyl chloride). *Polym. Degrad. Stab.* **2018**, *149*, 112−118.
(64) Park, K. S.; Ni, Z.; Côté, A. P.; Choi, J. Y.; Huang, R.; Uribe-Romo, F. J.; Chae, H. K.; O'Keeffe, M.; Yaghi, O. M. Exceptional chemical and thermal stability of zeolitic imidazolate frameworks. *Proc. Natl. Acad. Sci. U.S.A.* **2006**, *103* (27), 10186−10191.
(65) Priyadarsini, K. I.; Maity, D. K.; Naik, G.; Kumar, M. S.; Unnikrishnan, M.; Satav, J.; Mohan, H. Role of phenolic OH and methylene hydrogen on the free radical reactions and antioxidant activity of curcumin. *Free Radical Biol. Med.* **2003**, *35* (5), 475−484.
(66) Wright, J. S. Predicting the antioxidant activity of curcumin and curcuminoids. *J. Mol. Struct.: THEOCHEM* **2002**, *591* (1−3), 207−217.
(67) Prasad, E.; Hameeda, B.; Rao, A. B.; Reddy, G. Biotransformation of curcumin for improved biological activity and antiproliferative activity on acute HT-29 human cell lines 2014.
(68) Schreml, S.; Szeimies, R. M.; Karrer, S.; Heinlin, J.; Landthaler, M.; Babilas, P. The impact of the pH value on skin integrity and cutaneous wound healing. *J. Eur. Acad. Dermatol. Venereol.* **2010**, *24* (4), 373−378.
(69) Bennison, L.; Miller, C.; Summers, R.; Minnis, A.; Sussman, G.; McGuiness, W. The pH of wounds during healing and infection: a descriptive literature review. *Wound Pract. Res.* **2017**, *25* (2), 63−69.
(70) Plascencia Martinez, D. F.; Castillo, J. M. Q.; Orejarena, A. O.; Gallardo, A. P.; Merino, E. M.; López, G. A. T.; Peña, I. Y. L.; Martínez, D. H.; Gastelum, K. A. L.; Verduzco, A. A. L.; et al. Comparative Study of Single and Coaxial Electrospun Antimicrobial Cross-Linked Scaffolds Enriched with Aloe Vera: Characterization, Antimicrobial Activity, Drug Delivery, Cytotoxicity, and Cell Proliferation on Adipose Stem Cells and Human Skin Fibroblast. *ACS Omega* **2024**, *9* (40), 41157.
(71) Sethuraman, V.; Kishore, N.; Mohamed Saliq, A.; Loganathan, G.; Kandasamy, R. pH responsive metformin loaded zeolitic imidazolate framework (ZIF-8) for the treatment of lung cancer. *Mater. Technol.* **2022**, *37* (9), 926−934.
(72) Hoop, M.; Walde, C. F.; Riccò, R.; Mushtaq, F.; Terzopoulou, A.; Chen, X.-Z.; deMello, A. J.; Doonan, C. J.; Falcaro, P.; Nelson, B. J.; Puigmartí-Luis, J.; Pané, S. Biocompatibility characteristics of the metal organic framework ZIF-8 for therapeutical applications. *Appl. Mater. Today* **2018**, *11*, 13−21.
(73) Changmai, U.; K, L.; Mateti, T.; Kumari, M.; Savita; Narasimhaswamy, N.; Thakur, G. Evaluation of the Antibacterial Activity of Silver-Doped Curcumin-Loaded Zeolitic Imidazolate Framework-8 Against Methicillin-Sensitive and -Resistant *Staphylococcus aureus ChemRxiv* 2023 DOI: 10.26434/chemrxiv-2023-qx0q5.

https://doi.org/10.1021/acsomega.4c09945
ACS Omega 2025, 10, 3067−3079